Dynamic Trapping: Neutralization of Positive Space Charge in a Collisionless Magnetized Plasma

M. Bohm, N. Brenning, and C.-G. Fälthammar
Department of Plasma Physics, Royal Institute of Technology, Stockholm, Sweden
(Received 17 January 1990)

It is shown by numerical simulations that in a collisionless plasma electron inertia leads to inefficient neutralization of positive space charge and allows large positive potentials ($\phi \gg kT_e/e$) to be established and maintained on the time scale of ion motion. This is true even if the buildup of positive space charge is so slow that it corresponds to a small fraction of the random electron current of the surrounding plasma. A simple physical model clarifies the physics of the process and provides an analytical expression for the potential.

PACS numbers: 52.25.Wz

It is a fundamental characteristic of plasmas that any charge imbalance is opposed by electron displacements. Accordingly, classical theories predict that collisionless plasmas cannot support any significant magnetic-field-aligned electric-field components, because these will be quenched by electrons sliding freely along the field lines. The absence of significant magnetic-field-aligned electric fields is at the same time the condition for the magnetic field to be "frozen in," which has fundamental consequences for the dynamics of the plasma.

It is now known that magnetic-field-aligned electric fields do exist naturally in the collisionless space plasma and play a crucial role in the auroral process. They have also been observed in active experiments in the ionosphere.[1] Such fields can be supported by (1) the magnetic mirror force, as happens above the aurora, (2) wave turbulence, as in the case of anomalous resistivity, or (3) electron inertia, as in the case of double layers —for a review, see Fälthammar.[2]

In the present Letter we present a new mechanism that can support magnetic-field-aligned electric fields. Like the double layer it depends on electron inertia, but unlike the double layer is not limited to scales defined by the Debye length and it can support potentials much larger than kT/e without any net current. In a situation where a cross-field ion current needs to be neutralized by magnetic-field-aligned electron currents, this mechanism can led to incomplete neutralization and substantial magnetic-field-aligned electric fields. In this Letter we analyze the essential features of the mechanism by a numerical simulation. The physics involved is clarified by means of a simplified analytical treatment. Separate papers[1,3] elaborate on specific applications.

The code used in this simulation was constructed in a workshop at the University of California at Berkeley in 1983 and is called PDW1 (Plasma Device Workshop). PDW1 is a magnetized nonperiodic, electrostatic particle-in-cell code with one spatial coordinate along the magnetic field and three velocity coordinates. A more detailed description of the code is given by Lawson.[4] Because one application to our simulation is cross-field injections of heavy ions into the ionosphere we have chosen a background plasma with $kT_e = kT_i = 0.1$ eV, consisting of electrons and oxygens ions, and use the barium mass (137 amu) for the injected ions. We use the correct charge/mass ratio for all three species. The length of the system is $100\lambda_D$, where λ_D is the Debye length. The plasma is limited at $z=0$ and $z=L$ by two end plates with boundary conditions chosen to simulate a surrounding homogeneous plasma: Particles which hit the end plates are lost, and we inject half-Maxwellians at the end plates with the same temperature and density as the background plasma. The external circuit is chosen so that it gives the same potential $\phi(0)=\phi(L)=0$ on both end plates. In a region with a length of $L_{\rm inj}=30\lambda_D$ centered in the middle of the simulation region at $z=z_0$ the heavy ions are injected with a spatial distribution given by

$$R(z)=\frac{R_0}{2}\left[1+\cos\left(\frac{2\pi(z-z_0)}{L_{\rm inj}}\right)\right]. \quad (1)$$

$R(z)$ is the number of ions injected per time step and grid cell at the coordinate z, R_0 the number of particles injected per time step and grid cell at $z=z_0$, and $L_{\rm inj}$ the length over which the injection of heavy ions take place. R_0 can be varied in time in the simulation program. The buildup rate of the positive charge in a flux tube over the entire length of the injection region can then be compared to the random electron current across the end sections of the flux tube. A crucial value is the injection rate $R_0=R_{\max}$ at which saturation electron current is required along the magnetic field. $R_{\max}$ is then given by $R_{\max}=n_{e0}e(8kT_{e0}/\pi m_e)^{1/2}/L$.

In the simulation we use the normalized parameters: time $T=t\omega_{pe}$, potential $U=e\phi/kT_e$, and distance $Z=z/\lambda_D$. We have made three simulations with different injection rates, $R_0/R_{\max}=0.16$, 0.31, and 0.63. Figure 1 shows the temporal evolution of the potential in the simulation with $R_0/R_{\max}=0.31$. Between the plots there is a constant time difference $\Delta T=16$. The injection rate is gradually increased from $T=0$ to 40, and then kept constant. Thus there is, from the third plot, a constant increase in the density by approximately $\Delta(\Delta n_i)=n_{e0}/3$

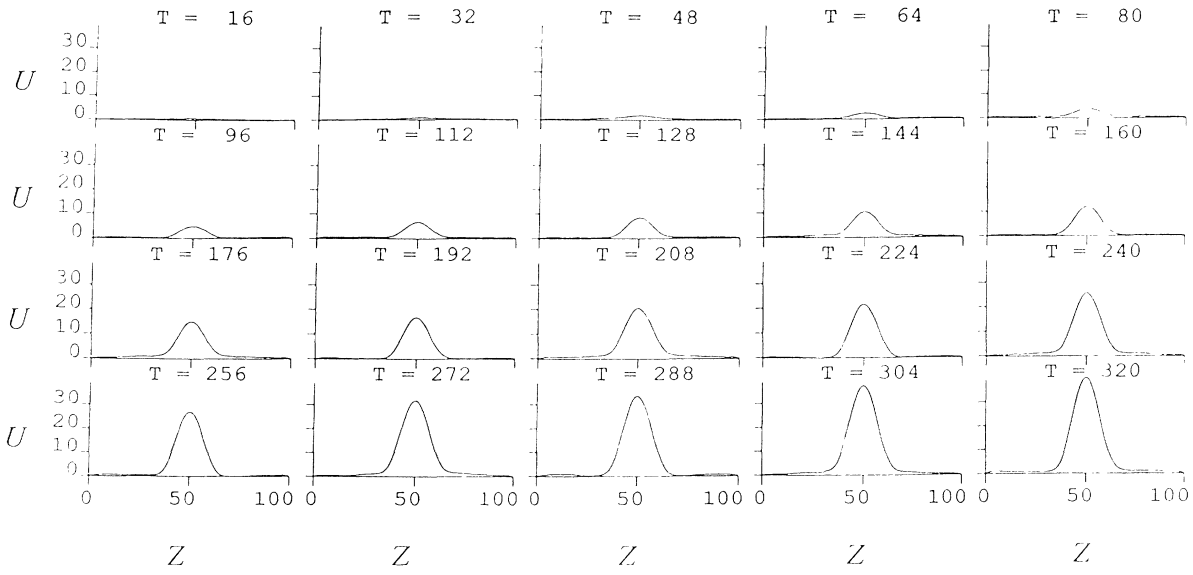

FIG. 1. The potential in the simulation region at different time steps. The units are normalized: $Z=z/\lambda_D$, $U=e\phi/kT_e$, and $T=t\omega_{pe}$. The injection rate is $R=0.31R_{\max}$, where $R_{\max}$ is the injection rate that requires electron saturation current along the magnetic field.

between the successive figures.

The positive potential in the injection region becomes larger than kT_{e0}/e as soon as the relative density increase exceeds unity. At the end of the run shown in Fig. 1, $\Delta n_i/n_{e0}\approx 5.7$ and $U\approx 40$. These high potentials are contained to the injection region, and show no sign of propagating into the ambient plasma. Consequently, there are very strong magnetic-field-aligned electric fields that surround the injected ions. These electric fields are independent of the current density, and even persist if the ion injection is switched off so that the current is zero.

Figure 2 shows detailed simulation results at $T=256$ with the same injection rate as in Fig. 1. The injected ions, which are shown in the top panel, have moved very little during the simulation time and remain close to their point of injection. The second panel shows the ambient ions which at $T=0$ had a uniform density. They are clearly beginning to move out of the injection region in response to the positive potential. The electrons (third panel) fill in the injection region so that quasineutrality is approximately maintained. The net charge is shown in panel number four: The positive space charge is incompletely neutralized and surrounded by negative space charges that screen it from the surroundings. The potential finally is shown in the bottom panel. It is closely limited to the region of ion injection.

Before we present more simulation results we will derive an analytical expression for the potential. As we are interested in electron time scales, the ions are considered stationary. Ions are added uniformly in the injection region from $-L/2$ to $L/2$. An electron which enters the injection region with a magnetic-field-aligned velocity v_{e0} has a transit time $t_{\text{transit}}=L/\langle v_e\rangle\approx L(2e\phi/m_e+v_{e0}^2)^{-1/2}$. It becomes trapped if the potential has grown more than $m_e v_{e0}^2/2e$ during the transit time. If ϕ increases much less than kT_{e0}/e during a typical electron transit time, then only the slowest electrons are trapped. If also $\phi > kT_{e0}/e$, then $v_{e0}^2 \ll 2e\phi/m_e$; the trapping condition becomes

$$v_{e0}^2 < 2L\left(\frac{2e}{m_e}\right)^{1/2}\frac{d}{dt}(\phi)^{1/2}. \tag{2}$$

We assume that the surrounding plasma has a Maxwell distribution with temperature T_{e0}. The influx of electrons that satisfy the condition (2) is found by integrating the Maxwell distribution up to that limit. The slowest electrons have a constant phase-space density $dn_e/dv=n_{e0}(m_e/2\pi kT_e)^{1/2}$, which yields

$$\frac{dN_e}{dt}=2L\left(\frac{2e}{m_e}\right)^{1/2}\frac{d}{dt}(\phi)^{1/2}n_{e0}\left(\frac{m_e}{2\pi kT_{e0}}\right)^{1/2}.$$

Integrating over time and introducing the average density increase $dn_e=dN_e/L$ we obtain the approximate density of trapped electrons:

$$n_{e,\,\text{trapped}}=n_{e0}(4e\phi/\pi kT_{e0})^{1/2}. \tag{3}$$

The free electrons start into the injection region with the average velocity $\langle|v_{e0}|\rangle=(2kT_{e0}/\pi m_e)^{1/2}$ and escape on the other side. At the potential ϕ they are accelerated to the average velocity $(2e\phi/m_e+\langle|v_{e0}|\rangle^2)^{1/2}$, and their density is reduced to

$$n_{e,\,\text{free}}=n_{e0}(1+\pi e\phi/kT_{e0})^{-1/2}.$$

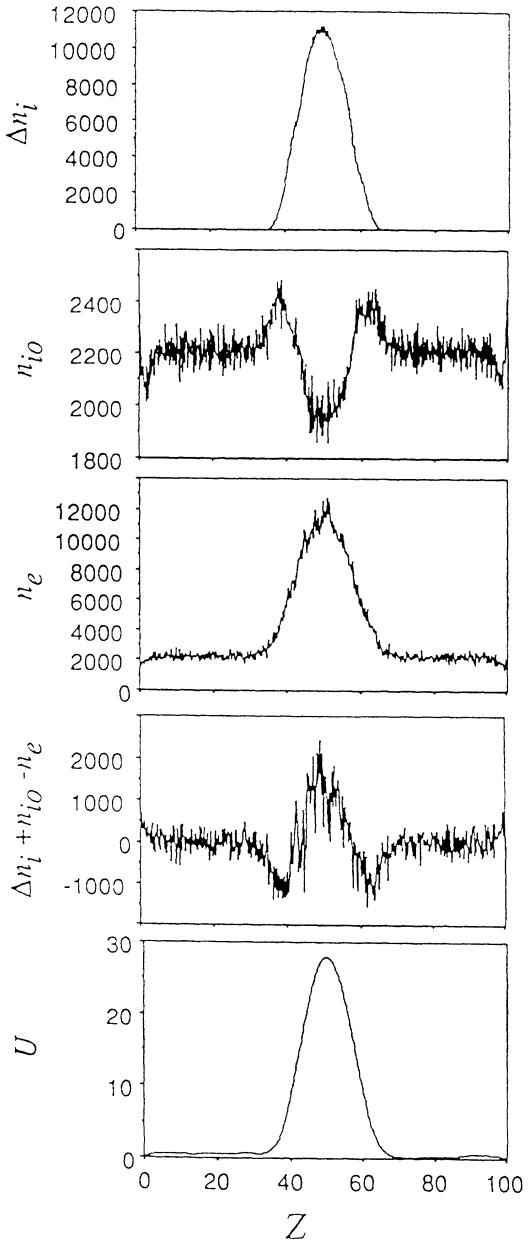

FIG. 2. From top to bottom: The injected ion density, the ambient ion density, the electron density, the net charge density, and the potential at time $T=256$ of Fig. 1.

The total electron density at potential ϕ is equal to the sum of the trapped and free electrons:

$$\frac{n_e}{n_{e0}} = \left(\frac{4e\phi}{\pi kT_{e0}}\right)^{1/2} + \left(1+\frac{\pi e\phi}{kT_{e0}}\right)^{-1/2}. \quad (4)$$

Since quasineutrality requires that $\Delta n_i \approx n_e - n_{e0}$, Eq. (4) gives the desired relation between the ion density increase and the potential. Notice that both L and dn_i/dt disappear in the final result. For high potentials, $\phi \gg kT_{e0}/e$, the free-electron density is small, $n_{e,\,\mathrm{free}} \ll n_{e0}$. Almost all the electrons then belong to the trapped

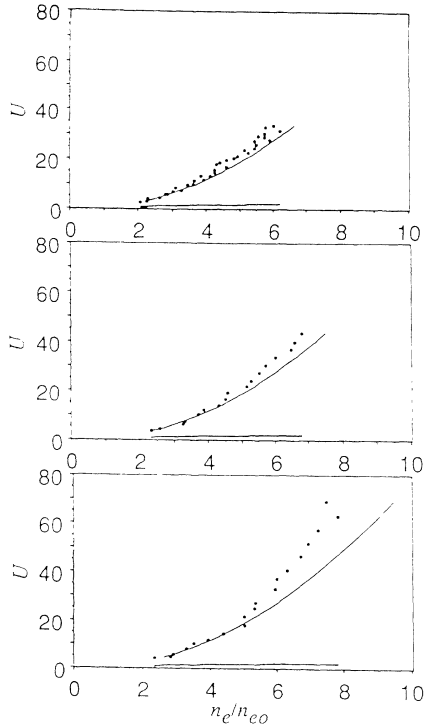

FIG. 3. The potential at $z=z_0$ vs n_e/n_{e0}. The dots are obtained from three computer simulations with different injection rates, from top to bottom: $R=0.16R_{\max}$, $0.31R_{\max}$, and $0.63R_{\max}$. The thin solid lines show the potential of the analytical theory, Eq. (4). For reference, the Boltzmann relation is shown as a thick solid line.

category and the potential is proportional to the square of the density according to Eq. (3).

It is interesting to compare this with the collisional case, where the relation between the density and the potential is given by the Boltzmann relation $n_e/n_{e0} = \exp(e\phi/kT_{e0})$. The crosses in Fig. 3 show the potential from the computer simulations versus the relative density increase n_e/n_{e0}, for the three different injection rates. The thin solid lines in Fig. 3 show Eq. (4), and the thick solid lines show the Boltzmann relation. When n_e/n_{e0} is large, the Boltzmann relation gives much lower potentials than the other calculations. For low-density increases, $\Delta n_i \approx n_{e0}$, the computer simulations and the other two calculations approach each other. Results at low-density increases are presented in a separate publication.[1] The agreement between Eq. (4) and the computer simulations is quite good. The largest discrepancy is obtained for the highest injection rate, shown in the bottom panel in Fig. 3, where the computed potentials exceed Eq. (4) by up to 40%. One possible reason is that Eq. (4) is derived under the approximation that only the central low-velocity part of the infalling electron distribution is trapped. This approximation becomes less valid for injection rates $R_0/R_{\max}$ that approach unity.

Another reason for the discrepancy between theory and simulation is that the theory assumes Maxwellian in-

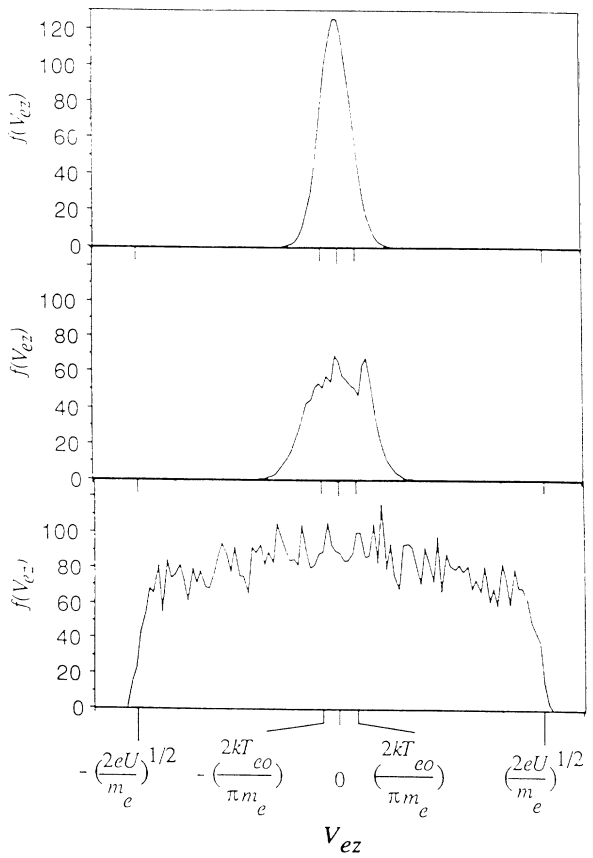

FIG. 4. Electron velocity distributions from the simulation shown in Fig. 1. Upper panel: The injected velocity distribution. Middle panel: The velocity distribution outside the injection region, averaged over 100 time steps around $T=336$. Bottom panel: The distribution at the center of the injection region at one time step, $T=336$.

falling electrons while in the simulation the electron distribution is modified by potential variations outside the injection region, which can be seen in Fig. 1. At the end plates there are sheaths with a potential difference of approximately kT_{e0}/e, and directed so that they accelerate the electrons into the simulation region. The amplitude of these sheaths stays approximately constant during each run with constant injection rate, but is different between the different runs; it increases with the injection rate. There is also a footpoint oscillation of the potential at the edge of the injection region, which is clearly seen between $T=192$ and 240. The frequency of this oscillation is not resolved here since it is higher than the sampling rate between the potential profiles.

Figure 4 shows the injected electron distribution at the end plates (upper panel) and also the distributions both outside the injection region at $Z=7$ (middle panel) and in the center of the cloud at $Z=50$ (bottom panel). These curves were made by division of the velocity space into cells with lengths of $dv=(v_{\max}-v_{\min})/100$ and the system length into cells with lengths of $dz=4\lambda_D$. For $Z=7$, the shape of the distribution varied rapidly in time, possibly due to the footpoint oscillations. In order to show the average infalling distribution towards the injection region we chose here to make an average over 100 time steps, centered at $T=336$. For $Z=50$, the bottom panel in Fig. 4 shows the distribution at one time step, $T=336$. The electron distribution outside the injection region can be qualitatively understood as a Maxwellian that has been modified by the end-plate sheaths.[2] The trapped distribution shown in the bottom panel of Fig. 3 is approximately a plateau in velocity space, with a phase-space density equal to the maximum of the injected Maxwellians at the end plates; according to Liouville's theorem this is the highest possible value in the absence of collisions. This plateau fills the whole velocity range between the velocity limits for trapped particles in a potential ϕ: $-(2e\phi/m_e)^{1/2}<v_{ez}<(2e\phi/m_e)^{1/2}$. Thus it seems that a growing potential as we have studied here automatically traps electrons at the highest rate that is physically possible for a given value of ϕ. The irregularities in the trapped electron distribution function could be due to the footpoint oscillations, which will modulate the velocity and density of the infalling electrons during the process of trapping.

In conclusion, we have demonstrated by one-dimensional computer simulations that a region where heavy ions are added across the magnetic field can attract and trap electrons along the magnetic field very efficiently also in the absence of collisions. In the process, the region gets a local positive potential which is proportional to the ambient electron temperature and to the square of the density, but independent both of the length of the injection region and of the rate of ion injection. The conditions for this result are that the density increase is larger than the ambient plasma density, and that the heavy ions are added at such a slow rate that space-charge neutrality can be maintained by magnetic-field-aligned currents below the electron saturation current. Very strong magnetic-field-aligned electric fields can by this process be maintained at low magnetic-field-aligned current densities.

This work has been financed by the Swedish Natural Science Research Council. We wish to thank Dr. I. Axnäs, Dr. M. A. Raadu, and Dr. S. Torvén for useful discussions and Dr. P. Gray for providing us with the code and for assistance with the numerical simulations.

[1]N. Brenning, M. Bohm, and C.-G. Fälthammar, Royal Institute of Technology, Division of Plasma Physics, Stockholm, Sweden, Report No. TRITA-EPP-89-07, 1989 (to be published).

[2]C.-G. Fälthammar, in *Proceedings of the ESA Workshop on Future Missions in Solar, Heliospheric and Space Physics, Garmisch-Partenkirchen, 30 April–3 May 1985* (European Space Agency Report No. SP 235, 107, 1985).

[3]M. Bohm, N. Brenning, and C.-G. Fälthammar (to be published).

[4]W. S. Lawson, J. Comput. Phys. **80**, 253 (1989).